Research article

NMR IN BIOMEDICINE

Received: 9 July 2012, Revised: 21 February 2013, Accepted: 22 February 2013, Published online in Wiley Online Library: 2013

(wileyonlinelibrary.com) DOI: 10.1002/nbm.2949

Mapping glutamate in subcortical brain structures using high-resolution GluCEST MRI

Kejia Cai[a]*, Anup Singh[a], David R. Roalf[b], Ravi Prakash Reddy Nanga[a], Mohammad Haris[a], Hari Hariharan[a], Ruben Gur[b] and Ravinder Reddy[a]

In vivo **measurement of glutamate (Glu) in brain subcortex can elucidate the role these structures play in cognition and neuropsychiatric disorders. However, accurate quantification of Glu in subcortical regions is challenging. Recently, a novel MRI method based on the Glu chemical exchange saturation transfer (GluCEST) effect has been developed for detecting brain Glu in millimolar concentrations. Here, we use GluCEST to map Glu distributions in subcortical structures of the human brain (e.g. amygdala, hippocampus). Overall, GluCEST was ~40% higher in gray matter than in white matter. Within the subcortical gray matters, amygdala showed the highest GluCEST contrast. Utilizing MR spectroscopic data, *in vivo* GluCEST detection sensitivity (~0.8% mM^{-1}) in subcortical gray matter was evaluated and was consistent with the previously reported values. In general, the GluCEST map approximates the Glu receptor distribution reported in previous positron emission tomography (PET) studies. These findings suggest that high-resolution GluCEST MRI of subcortical brain structures may prove to be a useful tool in diagnosis of brain disorders or treatment responses. Copyright © 2013 John Wiley & Sons, Ltd.**

Keywords: chemical exchange saturation transfer (CEST); glutamate; subcortical brain structures; amygdala; magnetic resonance spectroscopy (MRS)

INTRODUCTION

Glutamatergic dysfunction in the brain is implicated in cognitive deficits (1–3) and neuropsychiatric disorders including schizophrenia, Alzheimer's disease, drug abuse addiction and in autism depression (4). Thus, the demand for techniques that quantify and localize changes in brain glutamate (Glu) levels is high. This is of particular interest in subcortical brain regions, including the amygdala, hippocampus, caudate and putamen, as dysfunction in these regions affects cognition (5,6) and emotion processing (7) in various disorders.

Proton magnetic resonance spectroscopy (^{1}H-MRS) is one of the techniques used to assess potential disruptions in neuronal integrity and associated neurochemical dysregulations. While standard ^{1}H-MRS at 3 T allows for sufficient sensitivity to the neurochemistry in many regions of the brain, direct quantification of specific neurotransmitters such as Glu within small subcortical regions remains limited at this field strength (8,9). MRS at ultra-high field, 7 T (10), offers enhanced sensitivity due to higher Larmor frequency and the improved chemical shift dispersion, which enables better characterization of individual resonances (11).

Chemical exchange saturation transfer (CEST) MRI is a novel molecular imaging method that detects metabolites in millimolar (mM) concentration. For example, this technique has been used to quantify macromolecules based on the amide proton transfer (APT) effect (12,13), free calcium (14), starch hydrolysis and glucose mutarotation (15), liver glycogen (16), cartilage proteoglycan (17), and brain Glu with exchangeable amine protons (18). During CEST MRI, exchangeable protons are selectively irradiated by the application of a radio-frequency (RF) pulse. The exchange of saturated magnetization with bulk water protons results in reduced bulk water signal in a concentration and pH dependent manner. The CEST technique offers improved spatial resolution as compared with MR spectroscopic techniques due to the prolonged saturation process and the accumulation of an exchanging effect (18).

Previously employed APT methods (19,20) differentiate protein amide protons in gray and white matters, by showing higher APT effect in the white matter than the gray matter. For example, Dula *et al* (20) demonstrated that white-matter brain structures, such as splenium, have higher (~75%) APT contrasts than the gray-matter structures including caudate and putamen. Recently, we have demonstrated the feasibility of mapping Glu in healthy brain using the Glu amine proton CEST (GluCEST) effect (18). The notable difference between APT and GluCEST is the experimental conditions. In APT imaging, due to the low exchange rates of amide protons (~30 s^{-1}) associated with labile macromolecules and peptides, a lower saturation pulse amplitude (B_1 root mean

* *Correspondence to: Kejia Cai, University of Pennsylvania, Radiology, Philadelphia, PA, USA.*
E-mail: kcflying@gmail.com

a *K. Cai, A. Singh, R. P. R. Nanga, M. Haris, H. Hariharan, R. Reddy*
University of Pennsylvania, Radiology, Philadelphia, PA, USA

b *D. R. Roalf, R. Gur*
University of Pennsylvania, Psychiatry, Philadelphia, PA, USA

Abbreviations used: *^{1}H-MRS, proton magnetic resonance spectroscopy; APT, amide proton transfer; B_{1rms}, B_1 root mean square; CEST, chemical exchange saturation transfer; Glu, glutamate; GluCEST, glutamate chemical exchange saturation transfer; Glx, glutamate/glutamine; IRB, Institutional Review Board; mM, millimolar; NAA, N-acetylaspartate; PET, positron emission tomography; ppm, parts per million; PRESS, point-resolved spectroscopy; RF, radio-frequency; ROI, region of interest; SVS, single-voxel spectrum; T, Tesla; VAPOR, variable power RF pulses with optimized relaxation delays.*

square or $B_{1rms} = 50$ Hz (1.2 μT)) and longer duration (~6 s) were used (13) compared with GluCEST MRI ($B_{1rms} = 155$ Hz (3.6 μT) and 1 s). Using high-saturation B_1, faster-exchange (~2000 Hz) amine protons associated with Glu can be mapped using the GluCEST method. GluCEST has been demonstrated to differentiate Glu in gray and white matters by showing higher contrast in gray matter than in white matter (18).

This study is to further investigate whether GluCEST MRI can be used to map glutamate distributions in small subcortical gray-matter structures. In addition, we compare GluCEST contrast with the ^{1}H-MRS data to estimate the *in vivo* GluCEST detection sensitivity.

METHODS

All experiments were performed on a Siemens 7 T whole-body scanner with a vendor supplied 32-channel volume RF coil. The study was conducted under an approved Institutional Review Board (IRB) protocol.

GluCEST MRI

GluCEST MRI was acquired from six healthy male subjects (18–67 years old) using previously reported methods (18). T_1-weighted anatomical 3D magnetization prepared rapid gradient echo (MPRAGE) images of whole brain (160 axial slices) were collected using the following parameters: repetition time (TR)/echo time (TE) = 2110/3.2 ms, inversion time (TI) = 1.5 s, in-plan resolution = 0.9 × 0.9 mm^2 and slice thickness = 1 mm. The 3D reformatting of the MPRAGE images was used for selecting one axial and one sagittal slice for GluCEST imaging. The GluCEST imaging parameters were number of averages = 2, slice thickness = 5 mm, field of view = 200 × 200 mm^2, matrix size = 192 × 192, TR = 16 s. The saturation pulse train with 10 Hanning-windowed pulses (100 ms each, 99.8% duty cycle, B_{1rms} of 155 Hz or 3.6 μT) was followed by fast low-angle shot imaging (FLASH) readout (flip angle = 10°, readout TR/TE = 5.5/2.6 ms) of entire *K*-space. Raw CEST images were acquired at varying saturation offset frequencies ranging from ±2 to ±4 ppm (relative to water resonance) with a 0.25 ppm increment. To remove field inhomogeneity induced artifacts in GluCEST maps, images for B_1 and ΔB_0 field mapping were acquired and used for GluCEST reconstruction as previously described (17,18,21). In brief, CEST images obtained from ±2 to ±4 ppm were interpolated using the cubic spline method to generate images with a fine step size of 0.01 ppm. B_0 corrected CEST images at ±3 parts per million (ppm) were generated from the interpolated CEST images by picking signals according to the frequency shift in the ΔB_0 map. The B_0 corrected ±3.0 ppm images were then used for computing the percentage GluCEST contrast, which is equal to $100(M_{-3ppm} - M_{+3ppm})/M_{-3ppm}$, where M_{-3ppm} and M_{+3ppm} are B_0 corrected images at −3 ppm and +3 ppm respectively. B_1 inhomogeneity artifacts in GluCEST maps were removed using B_1 calibration curves as previously reported (21). The B_0 and B_1 corrected GluCEST contrasts were then averaged within expertly drawn regions of interest (ROIs). Overall, the acquisition of CEST images from one slice takes about 10 min. The acquisition of additional images required for mapping B_1 and B_0 field variation takes about 5 min.

MRS of glutamate

MRS data were collected from six healthy male subjects in a separated study. Localized manual shimming of the B_0 field

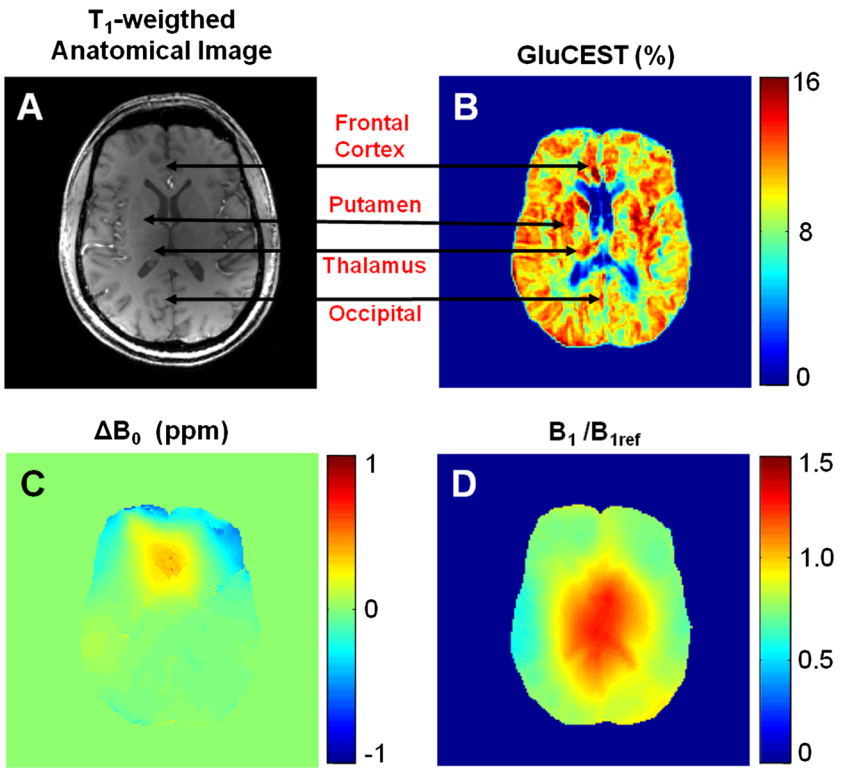

Figure 1. A representative GluCEST map from an axial brain slice. A, Proton anatomic image. C, ΔB_0 map; D, B_1 map (reference B_1 or $B_{1ref} = 155$ Hz or 3.6 μT); B, GluCEST map. Slight differences of CEST contrast in corresponding tissues across hemispheres may be due to brain positioning asymmetry.

NMR IN BIOMEDICINE

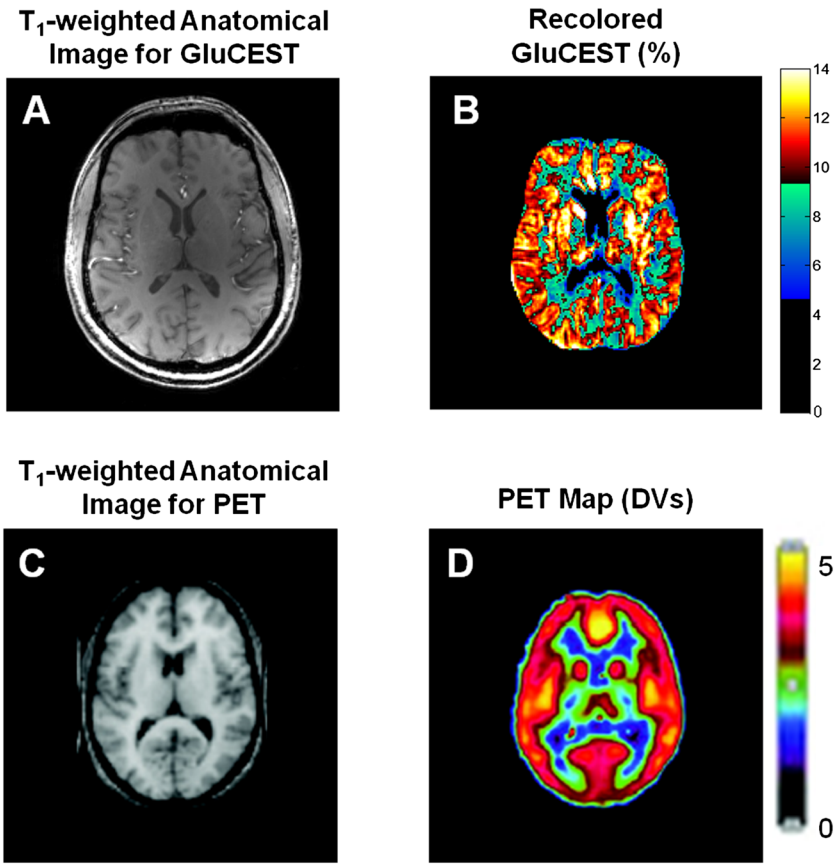

Figure 2. Comparison of GluCEST map with Glu receptor PET image. Proton anatomic image (A) and the corresponding GluCEST map (B). The recolored GluCEST map is reprocessed from Figure 1B by smoothing (2×2), rescaling and applying a colormap similar to the PET image, the combination of Black, 'Winter' and 'Hot' colormaps in MATLAB. Anatomic (T_1-weighted, C) and corresponding PET maps of distribution volumes (DVs) of metabotropic Glu receptor (D). *(Reprinted by permission of the Society of Nuclear Medicine: J. Nucl. Med. 31, Figure 2, copyright (2007).)* Although the GluCEST map and the PET image show similar patterns, their differences may due to differences in brain shapes, resolutions and slice thicknesses.

was performed in the left amygdala and hippocampus (voxel size: $10 \times 10 \times 10\,mm^3$) separately to obtain a localized water line width of ~0.15 ppm or less. Voxel placement was guided based on the 3D reformatting of high-resolution whole-brain MPRAGE images collected with the same parameters as above. Water suppressed short-echo single-voxel spectra (SVSs) were obtained with a custom-modified point-resolved spectroscopy (PRESS) sequence (22,23) to quantify Glu using parameters the following: spectral width = 4 kHz, number of points = 2048, averages = 128, TE = 20 ms and TR = 3 s. By changing the gradient ramp time and spoiler area, we were able to use a short TE of 20 ms. Water suppression was achieved with variable power RF pulses with optimized relaxation delays (VAPOR) (24), which was played out before the SVS acquisition. Acquisition time was ~6 min per spectrum. Water reference spectra were also acquired using the same sequence with water suppression turned 'off' and 16 averages. The total acquisition time for spectra from both voxels, structure scans and shimming was approximately 40 min.

We used custom-built spectroscopy processing packages developed in MATLAB (R2007b, MathWorks, Natick, MA, USA) for spectral processing, as recently reported (10). In brief, SVSs were processed from the raw free induction decay data by exponential apodization of 10 Hz, Fourier transformation, phase correction and baseline removal (25) followed by least-squared curve fitting. For Glu quantification, water suppressed SVSs were fitted as a sum of Gaussian peaks initially positioned at locations corresponding to brain metabolites. The integration of the 2.35 ppm Glu peak was normalized by a water reference signal for Glu quantification.

Statistical analysis

Two-tailed paired Student's *t*-tests were used to compare GluCEST contrasts and Glu quantifications using ^{1}H-MRS in different brain structures. The difference is considered to be significant for $p < 0.05$.

RESULTS

A high-resolution GluCEST map of an axial brain slice corrected for B_0 and B_1 inhomogeneities is shown in Figure 1B. The ΔB_0 map (Figure 1C) of this slice generally shows ~0.5 ppm variations and the B_1 map (Figure 1D) less than 50% of variance compared with the reference B_1 (B_{1ref}). The GluCEST map (Figure 1B) shows higher GluCEST in subcortical structures, such as putamen, caudate and thalamus, than cortex and occipital gray matters. White matter has much lower contrast than all gray-matter tissues and negligible contrast is seen from the cerebrospinal fluid (CSF). The spatially smoothed GluCEST map shown in Figure 2B approximates the PET volume distribution map of glutamate

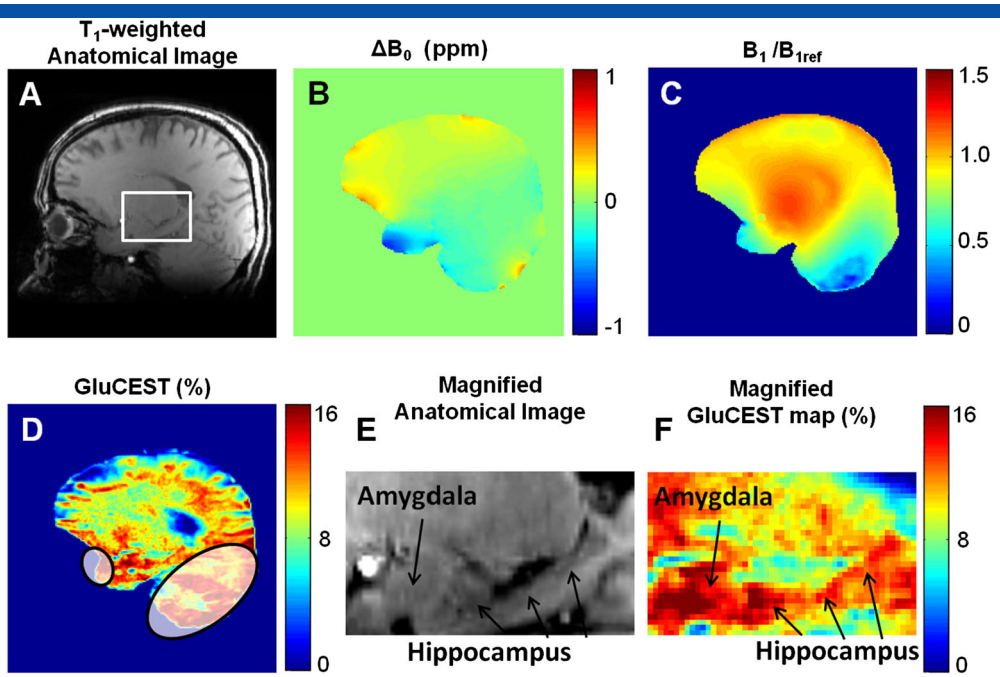

Figure 3. A representative GluCEST map from a sagittal brain slice. Representative MRI data from sagittal brain slice. A, Proton anatomic image showing amygdala and hippocampus in the white box. B, ΔB_0 map; C, B_1 map; D, GluCEST map of the same slice. Two regions marked with ovals have less than 50% B_1 that cannot be fully corrected for B_1 inhomogeneity. E,F, A 15 times magnification of the proton image and CEST map from the amygdala and hippocampus region (white square in A).

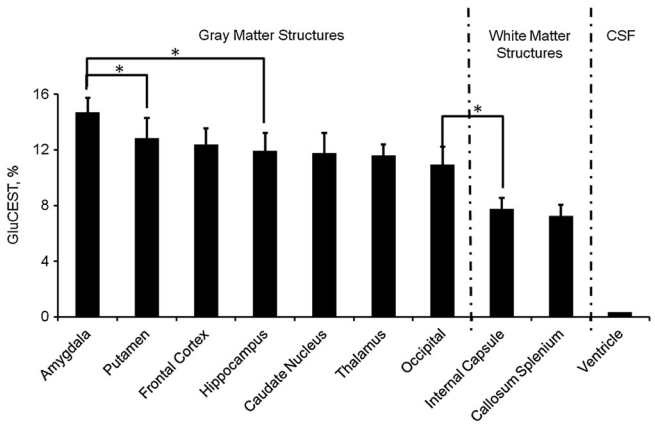

Figure 4. Regional variation of average ($n = 6$) GluCEST contrast from different brain structures. The observed GluCEST is about 40% higher in gray matter, such as putamen and occipital lobe, than in white-matter regions, such as internal capsule and callosum splenium. GluCEST in amygdala is significantly higher than that in other gray matters (*$p < 0.05$), which is significantly higher than that in white-matter regions (e.g. internal capsule).

receptor (26) (Figure 2D), despite differences in brain shape (Figure 2A *versus* 2C), resolution and sensitivity, demonstrating the ability of GluCEST MRI to map the regional distribution of Glu in the brain.

High-resolution GluCEST imaging was also performed for a sagittal brain slice containing amygdala and hippocampus structures (Figure 3). The ΔB_0 map (Figure 3B) of this slice generally shows variation within the interval (−1, 1) ppm and the B_1 map (Figure 3C) shows less than 50% variation in most regions of the brain despite the area around cerebellum and a small portion of the frontal lobe. Due to the large B_1 inhomogeneity, the B_1 inhomogeneity induced artifact in the GluCEST map (Figure 3D) cannot be fully corrected in these two regions (masked with ovals). The magnified GluCEST map (Figure 3F) from the amygdala–hippocampus region shows higher contrast from amygdala than hippocampus.

The summarized mean GluCEST contrast of the subcortical structures is shown in Figure 4. Amygdala shows the highest contrast ($15 \pm 1\%$) in all the gray-matter structures, which is significantly higher than that of hippocampus ($12 \pm 1\%$). Consistent with previous reports (18), white-matter tissue has about 40% less contrast than most gray-matter tissues. The GluCEST regional distribution approximates to glutamate spatial variations quantified by ^{1}H-MRS (27).

A modified PRESS based SVS sequence using short TE down to 20 ms was successfully implemented in the subcortex at 7 T. Using a 32-channel head coil, we were able to obtain water suppressed spectra from amygdala and hippocampus with 1 cc voxel size and adequate signal to noise ratio (Figures 5 and 6). The Glu peak located at 2.35 ppm is clearly visible and well separated from *N*-acetylaspartate (NAA) at 2 ppm. Glu concentration quantified from MRS was higher in amygdala as compared with hippocampus (Figures 5 and 6). Mean Glu concentration (Figure 5B) was 17 ± 3 mM in the amygdala and 14 ± 3 mM in the hippocampus. These values are comparable to those in a recent study at 3 T (8). The differences of GluCEST contrast and Glu concentration quantified by MRS between amygdala and hippocampus are $2.8 \pm 1.3\%$ and 3.4 ± 2.0 mM respectively, giving a GluCEST detection sensitivity of ~0.8% per mM *in vivo*, which is close to the previously reported 0.77% mM^{-1} in gray matter (18).

NMR IN BIOMEDICINE

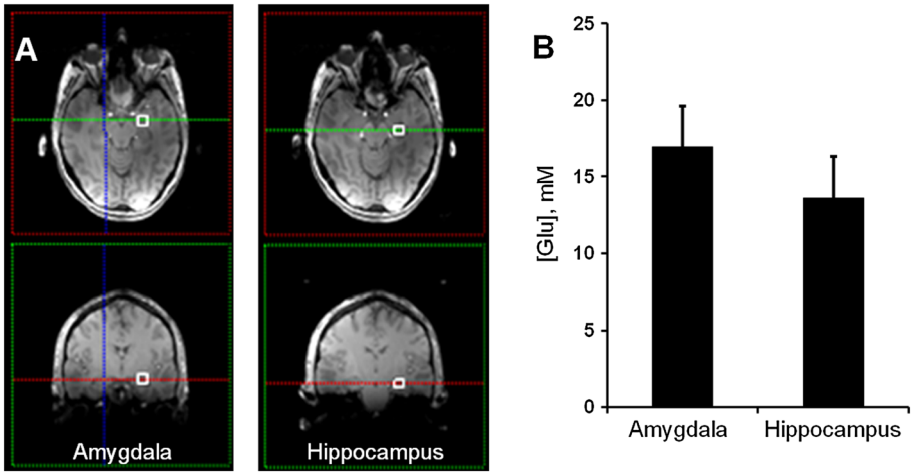

Figure 5. A, Anatomic images in axial (top) and coronal (bottom) axis used for prescribing amygdala and hippocampus voxels (white squares) for MRS. B, Averaged (±SD) concentrations of Glu obtained using ^{1}H-MRS in amygdala and hippocampus.

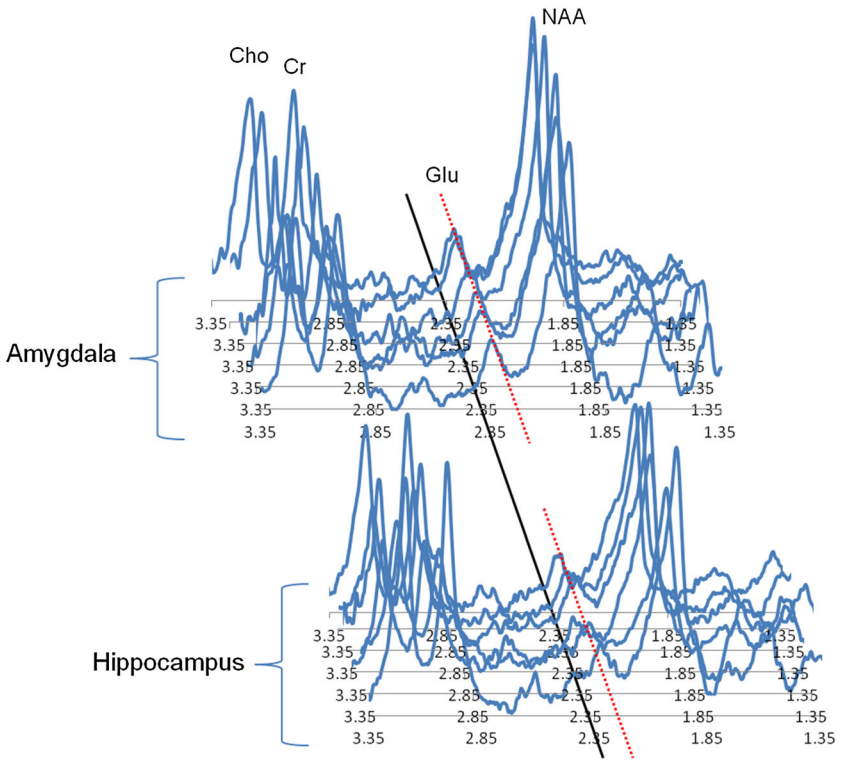

Figure 6. Stack plots of all the MR spectra collected from amygdala (top) and hippocampus (bottom) at 7 T. The black line was used for lining up all the spectra and the red dotted lines were placed approximately on the averaged peak height of the glutamate peak at 2.35 ppm.

DISCUSSION

Subcortical Glu was measured using 7 T ^{1}H-MRS and CEST MRI, a novel alternative molecular imaging method that has been recently utilized for detecting metabolites in millimolar concentration. The Glu peak at 2.35 ppm was clearly resolvable using ^{1}H-MRS and the concentration of Glu was higher in the amygdala than the hippocampus. Consistently, the observed GluCEST is about 40% higher in gray matter than in white matter. Within gray-matter structures, amygdala shows the highest GluCEST contrast, which is consistent with previous findings that amygdala has the highest ratio of relative regional cerebral blood flow to glucose metabolism in the brain (28). GluCEST maps also show a similar distribution pattern as compared with PET maps of the Glu receptor (26). Comparing GluCEST regional variation with glutamate concentrations quantified using ^{1}H-MRS, we estimate the *in vivo* GluCEST detection sensitivity of 0.8% mM^{-1} in gray matters. This is consistent with the previous estimation based on numerical simulations of full Bloch–McConnell equations (18). Taken together, these data provide

additional evidence that Glu in subcortical structures is measurable using GluCEST MRI.

In our previous study (18), a superficial brain slice in the axial view was scanned to demonstration the feasibility of GluCEST MRI for differentiating glutamate levels in gray and white matter. Here, we extend upon these findings to map glutamate distribution in the brain subcortex. Importantly, neurochemical dysfunction within subcortical structures is often implicated in neuropsychiatric and neurodegenerative disorders. For example, the amygdala facilitates perception of salient stimuli and is associated with social/emotional processing and emotional learning, which is affected in schizophrenia (29). Moreover, schizophrenia is associated with persistent dysfunction of Glu transmission (30). Given the importance of the subcortical structures in emotion, memory and other behavioral domains, accurate quantification of the neurochemicals and neurotransmitters via GluCEST may prove useful in improving diagnosis specificity or quantifying treatment response.

However, a few issues must be considered. Precise quantification of Glu from short-echo MRS remains a challenge due to overlapping signal from macromolecules (31,32). While GluCEST MRI may be more suitable for molecular imaging of brain glutamate, GluCEST detection sensitivity is field dependent and varies with tissue pH and imaging parameters, including RF saturation power and duration.

Direct conversion of GluCEST contrast into absolute concentration remains a challenge because GluCEST contrast as 3 ppm may have contributions from creatine, gamma-aminobutyric acid (GABA), amide protons and intrinsic magnetic transfer asymmetry as discussed previously (18). Furthermore, using *in vitro* experiments of denatured protein solutions to estimate *in vivo* conditions (e.g. exchange rates) may not be analogous. Based upon the numerical simulations of full Bloch–McConnell equations (18), we estimate that glutamate is the major contributor to the observed GluCEST. However, more work is needed to precisely determine the amount of contamination from other factors.

Finally, successful implementation of GluCEST in some brain regions remains challenging as CEST MRI is vulnerable to B_0 and B_1 field inhomogeneities, and proper correction (17,18,21) is required to precisely determine GluCEST contrast. In this study, the use of a saturation offset range larger than the actual B_0 variation ensures that GluCEST can be fully corrected for B_0 inhomogeneity. However, there are substantial B_1 inhomogeneities (up to more than 50%) in the sagittal acquisition that cannot be fully corrected using calibration based methods (21). Hence, caution should be exercised when interpreting the data from regions with large B_1 variation.

In conclusion, given the consistency of subcortical GluCEST contrasts with PET and MRS studies, GluCEST mapping may serve as a biomarker of brain Glu distribution *in vivo*. High-resolution GluCEST MRI could help elucidate normal brain function and improve diagnosis of neural disorders associated with dysfunction of subcortical structures.

Acknowledgements

This work was supported by the National Center for Research Resources and the National Institute of Biomedical Imaging and Bioengineering of the National Institutes of Health through grant P41 EB015893 and grants R21-DA032256, R01-MH060722, P50-MH064045 and T32 MH019112.

REFERENCES

1. Buckley PF, Moore C, Long H, Larkin C, Thompson P, Mulvany F, Redmond O, Stack JP, Ennis JT, Waddington JL. 1H-magnetic resonance spectroscopy of the left temporal and frontal lobes in schizophrenia: clinical, neurodevelopmental, and cognitive correlates. Biol. Psychiatry 1994; 36(12): 792–800.
2. Modrego PJ, Fayed N, Pina MA. Conversion from mild cognitive impairment to probable Alzheimer's disease predicted by brain magnetic resonance spectroscopy. Am. J. Psychiatry 2005; 162(4): 667–675.
3. Zahr NM, Mayer D, Pfefferbaum A, Sullivan EV. Low striatal glutamate levels underlie cognitive decline in the elderly: evidence from in vivo molecular spectroscopy. Cereb. Cortex 2008; 18(10): 2241–2250.
4. Javitt DC, Schoepp D, Kalivas PW, Volkow ND, Zarate C, Merchant K, Bear MF, Umbricht D, Hajos M, Potter WZ, Lee CM. Translating glutamate: from pathophysiology to treatment. Sci. Transl. Med. 2001. DOI: 10.1126/scitranslmed.3002804
5. Strange BA, Dolan RJ. Anterior medial temporal lobe in human cognition: memory for fear and the unexpected. Cogn. Neuropsychiatry 2006; 11(3): 198–218.
6. Zimmerman ME, Brickman AM, Paul RH, Grieve SM, Tate DF, Gunstad J, Cohen RA, Aloia MS, Williams LM, Clark CR, Whitford TJ, Gordon E. The relationship between frontal gray matter volume and cognition varies across the healthy adult lifespan. Am. J. Geriatr. Psychiatry 2006; 14(10): 823–833.
7. Calder AJ, Keane J, Manes F, Antoun N, Young AW. Impaired recognition and experience of disgust following brain injury. Nat. Neurosci. 2000; 3(11): 1077–1078.
8. Nacewicz BM, Angelos L, Dalton KM, Fischer R, Anderle MJ, Alexander AL, Davidson RJ. Reliable non-invasive measurement of human neurochemistry using proton spectroscopy with an anatomically defined amygdala-specific voxel. Neuroimage 2011; 59(3): 2548–2559.
9. Brierley B, Shaw P, David AS. The human amygdala: a systematic review and meta-analysis of volumetric magnetic resonance imaging. Brain Res. Rev. 2002; 39(1): 84–105.
10. Cai K, Nanga RP, Lamprou L, Schinstine C, Elliott M, Hariharan H, Reddy R, Epperson CN. The impact of gabapentin administration on brain GABA and glutamate concentrations: a 7 T (1)H-MRS study. Neuropsychopharmacology 2012; 37(13): 2764–2771.
11. Choi C, Dimitrov IE, Douglas D, Patel A, Kaiser LG, Amezcua CA, Maher EA. Improvement of resolution for brain coupled metabolites by optimized (1)H MRS at 7T. NMR Biomed.. 2010; 23(9): 1044–1052.
12. Zhou J, Lal B, Wilson DA, Laterra J, van Zijl PC. Amide proton transfer (APT) contrast for imaging of brain tumors. Magn. Reson. Med. 2003; 50(6): 1120–1126.
13. Zhou J, Payen JF, Wilson DA, Traystman RJ, van Zijl PC. Using the amide proton signals of intracellular proteins and peptides to detect pH effects in MRI. Nat. Med. 2003; 9(8): 1085–1090.
14. Gilboa H, Chapman BE, Kuchel PW. 19F NMR magnetization transfer between 5-FBAPTA and its complexes. An alternative means for measuring free Ca^{2+} concentration, and detection of complexes with protein in erythrocytes. NMR Biomed.. 1994; 7(7): 330–338.
15. Dona AC, Pages G, Kuchel PW. Kinetics of starch hydrolysis and glucose mutarotation studied by NMR chemical exchange saturation transfer (CEST). Carbohydr. Polym. 2011; 86(4): 1525–1532.
16. van Zijl PC, Jones CK, Ren J, Malloy CR, Sherry AD. MRI detection of glycogen in vivo by using chemical exchange saturation transfer imaging (glycoCEST). Proc. Natl. Acad. Sci. USA 2007; 104(11): 4359–4364.
17. Singh A, Haris M, Cai K, Kassey VB, Kogan F, Reddy D, Hariharan H, Reddy R. Chemical exchange saturation transfer magnetic resonance imaging of human knee cartilage at 3 T and 7 T. Magn. Reson. Med. 2012; 68(2): 588–594.
18. Cai K, Haris M, Singh A, Kogan F, Greenberg JH, Hariharan H, Detre JA, Reddy R. Magnetic resonance imaging of glutamate. Nat. Med. 2012; 18(2): 302–306.
19. Zhou J, Blakeley JO, Hua J, Kim M, Laterra J, Pomper MG, van Zijl PC. Practical data acquisition method for human brain tumor amide proton transfer (APT) imaging. Magn. Reson. Med. 2008; 60(4): 842–849.
20. Dula AN, Asche EM, Landman BA, Welch EB, Pawate S, Sriram S, Gore JC, Smith SA. Development of chemical exchange saturation transfer at 7 T. Magn. Reson. Med. 2011; 66(3): 831–838.
21. Singh A, Cai K, Haris M, Hariharan H, Reddy R. On B(1) inhomogeneity correction of in vivo human brain glutamate chemical exchange

saturation transfer contrast at 7T. Magn. Reson. Med. 2012. DOI: 10.1002/mrm.24290
22. Hoshino Y, Yoshikawa K, Inoue Y, Asai S, Nakamura T, Ogino T, Umeda M, Iwamoto A. Reproducibility of short echo time proton magnetic resonance spectroscopy using point-resolved spatially localized spectroscopy sequence in normal human brains. Radiat. Med. 1999; 17(2): 115–120.
23. van der Graaf M, Jager GJ, Heerschap A. Removal of the outer lines of the citrate multiplet in proton magnetic resonance spectra of the prostatic gland by accurate timing of a point-resolved spectroscopy pulse sequence. MAGMA 1997; 5(1): 65–69.
24. Tkac I, Starcuk Z, Choi IY, Gruetter R. In vivo ^{1}H NMR spectroscopy of rat brain at 1 ms echo time. Magn. Reson. Med. 1999; 41(4): 649–656.
25. Cobas JC, Bernstein MA, Martin-Pastor M, Tahoces PG. A new general-purpose fully automatic baseline-correction procedure for 1D and 2D NMR data. J. Magn. Reson. 2006; 183(1): 145–151.
26. Ametamey SM, Treyer V, Streffer J, Wyss MT, Schmidt M, Blagoev M, Hintermann S, Auberson Y, Gasparini F, Fischer UC, Buck A. Human PET studies of metabotropic glutamate receptor subtype 5 with 11C-ABP688. J. Nucl. Med. 2007; 48(2): 247–252.
27. Michaelis T, Merboldt KD, Bruhn H, Hanicke W, Frahm J. Absolute concentrations of metabolites in the adult human brain in vivo: quantification of localized proton MR spectra. Radiology 1993; 187 (1): 219–227.
28. Gur RC, Ragland JD, Reivich M, Greenberg JH, Alavi A, Gur RE. Regional differences in the coupling between resting cerebral blood flow and metabolism may indicate action preparedness as a default state. Cereb. Cortex 2009; 19(2): 375–382.
29. Phelps EA, LeDoux JE. Contributions of the amygdala to emotion processing: from animal models to human behavior. Neuron 2005; 48(2): 175–187.
30. Olney JW, Farber NB. Glutamate receptor dysfunction and schizophrenia. Arch. Gen. Psychiatry 1995; 52(12): 998–1007.
31. Mader I, Seeger U, Karitzky J, Erb M, Schick F, Klose U. Proton magnetic resonance spectroscopy with metabolite nulling reveals regional differences of macromolecules in normal human brain. J. Magn. Reson. Imaging 2002; 16(5): 538–546.
32. Kassem MN, Bartha R. Quantitative proton short-echo-time LASER spectroscopy of normal human white matter and hippocampus at 4 Tesla incorporating macromolecule subtraction. Magn. Reson. Med. 2003; 49(5): 918–927.